Preprint Title	Vibrations of organic nanofibres in a solvated bis-imidazolium supramolecular hydrogel
Authors	Daniela Dupkalova, David B. Amabilino and Lluïsa Pérez-García
Publication Date	10 Sept. 2026
Article Type	Full Research Paper
Supporting Information File 1	Article BJNANO_DD_nanoscale vibration SI.pdf; 1.3 MB
Supporting Information File 2	Intensity-4p-10fps.mp4; 96.4 MB
Supporting Information File 3	Intensity-6p-10fps.mp4; 92.2 MB
Supporting Information File 4	Intensity-8p-10fps.mp4; 88.4 MB
ORCID® iDs	Daniela Dupkalova - https://orcid.org/0009-0009-9371-3731; David B. Amabilino - https://orcid.org/0000-0003-1674-8462; Lluïsa Pérez-García - https://orcid.org/0000-0003-2031-4405

Vibrations of organic nanofibres in a solvated bis-imidazolium supramolecular hydrogel

Daniela Dupkalová[1,2], David B. Amabilino*[3] and Lluïsa Pérez-García*[1,2]

Addresses:

[1] Departament de Farmacologia, Toxicologia i Química Terapèutica, Facultat de Farmàcia i Ciències de l'Alimentació, Avda. Joan XXIII 27-31, Universitat de Barcelona, 08028 Barcelona, Spain

[2] Institut de Nanociència i Nanotecnologia IN2UB, Universitat de Barcelona, Barcelona, 08028 Spain

[3] Institut de Ciència de Materials de Barcelona (ICMAB-CSIC), Carrer dels Til·lers, Cerdanyola del Vallès, 08193 Spain.

ORCID identifiers:

Daniela Dupkalová 0009-0009-9371-3731

David B. Amabilino 0000-0003-1674-8462

Lluïsa Pérez-García 0000-0003-2031-4405

* Corresponding author

Email: David Amabilino – amabilino@icmab.es Lluïsa Pérez-García – mlperez@ub.edu

Abstract

A multicomponent supramolecular hydrogel based on a gemini imidazolium gelator that forms fibres incorporating anionic azobenzene and porphyrin derivatives, that absorb violet light, is shown to exhibit vibrations of the self-assembled fibres. Apparently not observed previously, it is found that in regions of the hydrated gel with low fibre concentration the fibres move perpendicularly to their long axis when observed using total internal reflection fluorescence microscopy and a monochromatic light source to excite the porphyrin. The movement is shown to be robust, in that it is continuous up to at least 300 seconds without any breakage of the fibres. The vibrational frequency and amplitude are independent of the laser intensity within the used range of photon flux, indicating that the vibrations originate from bulk thermal motion. The bulk gel that has many fibre interconnections does not show any fibre movement. Therefore, the vibrations are assumed to be manifested because of a relatively small number of fibre connections within gel network. The thermal energy and consequent Brownian motion of the surrounding bulk liquid are believed to be the power source that drives these motions.

Keywords

Colloid; fluorophore; microscopies; organic nanofibre; supramolecular hydrogel.

Introduction

Supramolecular hydrogels are soft materials formed by self-assembly of low molecular weight gelators to give nanoscopic fibres held together by reversible non-covalent interactions that are responsible for gel formation [1-3]. Upon studying potential use of supramolecular hydrogels in environmental, technological, and biomedical applications, a great number of gel systems with unique physicochemical properties have been prepared [4-9]. Most of these studies concentrate on the interactions between the gelators, as this is the principle driving force for the formation of the fibres that lead to the networks [10-12], although the weak interactions between gel fibres that hold the networks together have not generally been explored at the nanoscopic individual fibre level. It is known that the topological nature of the network's microstructure is supersaturation dependent [13].

Understanding interactions of the system's components at the molecular level is crucial for tailoring the properties, such as swelling behaviour, viscoelasticity, biocompatibility, and self-healing capability, that makes them a promising material for energy storage applications [7,8], and a wide range of biomedical applications such as tissue engineering [14], and therapeutic delivery [15]. We have shown that supramolecular hydrogels based on gemini imidazolium amphiphiles like the gelator **1**·2Br (Fig. 1) can be used for drug delivery [16-18], singlet oxygen generation [19, 20], and antimicrobial photodynamic therapy [21]. The gel system based on **1**·2Br incorporating 5,10,15,20-tetrakis(4-carboxyphenyl)porphyrin (TCPP; Fig. 1) and 4-(phenylazo)benzoic acid (**Azo**; Fig. 1) is a light-responsive system [22]. Irradiation of the gel with 405 nm light causes excitation of both **TCPP** and **Azo**, leading to fluorescence of the porphyrin and the simultaneous isomerization of the **Azo** photoswitch. The energy absorption and isomerisation allows **TCPP** to overcome its local electrostatic interactions and disturb

the gel fibre in which it is incorporated, leading to **TCPP** movement along the path of fibres of **1**·2Br. In the **1**·2BrGel@**TCPP**@**Azo** system prepared with 1:1 water:ethanol volume ratio, **TCPP** movement is always oriented away from an irradiated area.

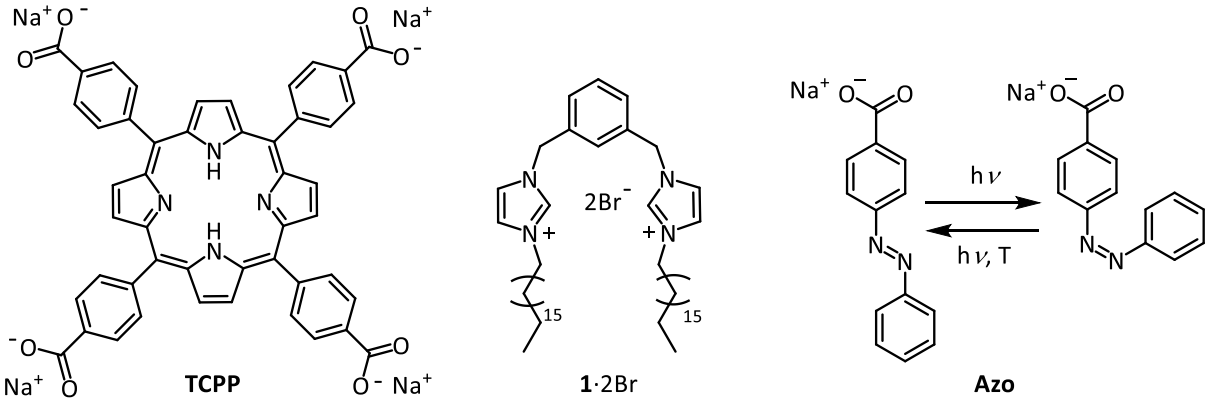

Figure 1: Chemical structures of **TCPP**, **1**·2Br and **Azo** molecules.

As **1**·2BrGel@**TCPP**@**Azo** formation is governed by far-from-equilibrium self-assembly resulting from the mixing of solutions of distinct composition, formation of a fibre network with a significant amount of inhomogeneity at the microscopic level is inevitable. In this work we explore some of these regions of varying morphology, showing that where the gel fibre concentration is lower, and therefore the fibres are not as interconnected as in more concentrated regions, vibrations of fibres were observed. We describe here the analysis of the fibre vibrations and explore the relationship between the properties of the vibrations and the laser intensity of the irradiation.

Results and Discussion

Observation of fibre vibration

The hydrogels formed here are made by the so-called “solvent-switch” method, where water and ethanol are used to dissolve completely components of the gel (**TCPP** in water and **1**·2Br and **Azo** in ethanol) and, upon mixing, the solutes begin to self-assemble forming the fibre network over varying amounts of time (from seconds to hours) [22]. After mixing, the sample was immediately pipetted into the microscope slide’s wells where the gel formed, and at least 12 hours prior to imaging. Speed of gel formation strongly depends on the temperature [23]. In the present case, use of 23 °C solutions ensured gel formation is completed within minutes.

Total internal reflection fluorescence (TIRF) microscopy has been used here to observe the gels. It has advantages over other imaging techniques because, provided a fluorophore is present, the fibres can be observed in the liquid that comprises most of gel volume and a very shallow depth of the sample can be imaged, very close to the interface between the glass slide and the sample. In the present study, the penetration depth set on the microscope was generally 60 nm from the glass slide-sample interface, that corresponds to an angle of reflection of 71°. The gels appear largely as before [19, 22], where a network of straight and slightly curved fibres is observed. Inhomogeneities are apparent, where dense fibre conglomerates are seen in some places, while in other regions the fibre density is relatively low, with representative regions shown in Figure 2.

All fibres analysed here were recorded under the same conditions. It should be noted that with most analysis techniques (such as atomic force microscopy or scanning electron microscopy [24]), it is not possible to see these inhomogeneities, either because they are ensemble measurements or because the analysis is performed on

dried samples. At least some collapse of the sample is possible under those conditions. Using TIRF microscopy, the gel fibres are observed in their solvated state, surrounded by solvent, using a moderate-intensity laser light that in the present case does not affect the structure of the sample over the time taken to record the measurements.

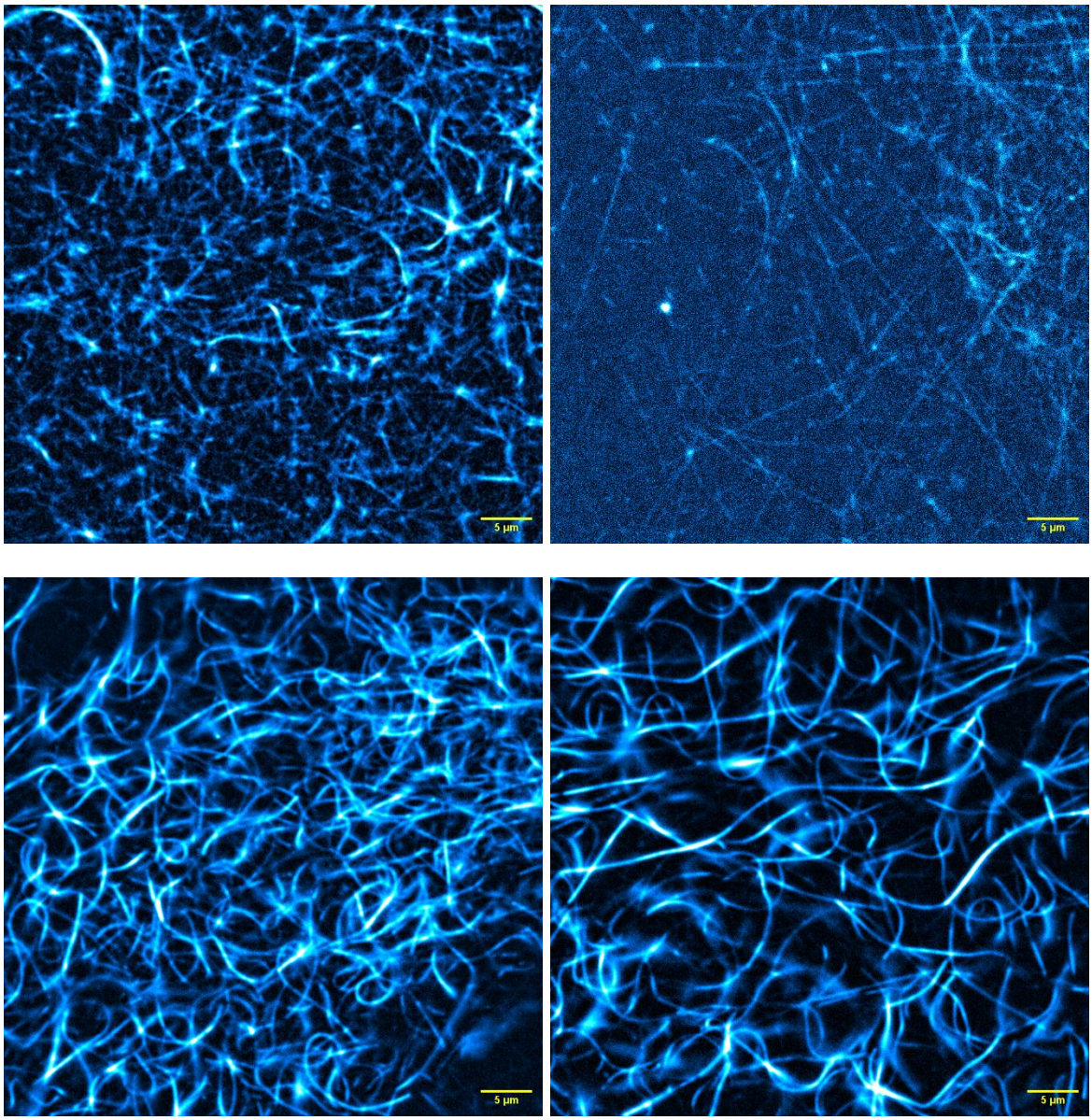

Figure 2: TIRF images (4% laser intensity, penetration depth 60 nm) of representative regions of the **1**·2BrGel@**TCPP**@**Azo** gel in 1:1 water:ethanol showing the variety of local environments.

In regions of relatively low fibre density, where separate individual fibres are clearly seen with a large distance between crossing points, it was possible to observe single fibres moving from side to side. The rate of this movement is slow on the timescale of recording of the images (100 milliseconds). Figure 3 shows still images of this kind of event. This vibration was only observed in these low-density regions and not where a greater number of fibres per unit area were seen in the sample.

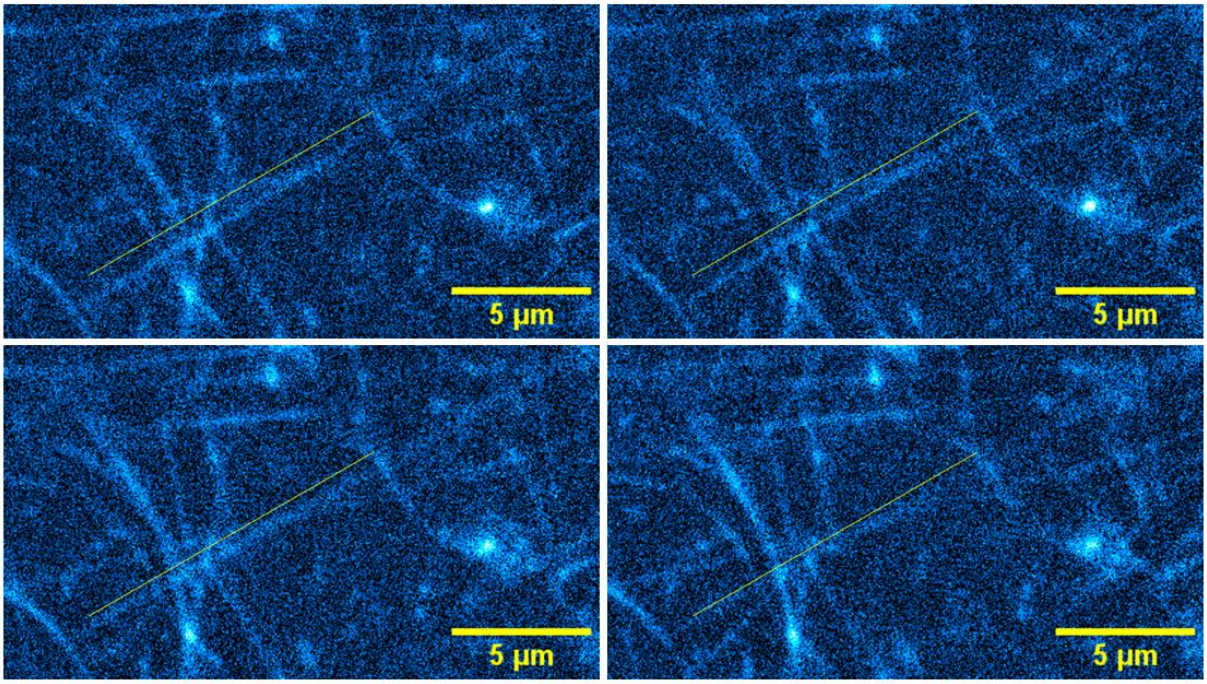

Figure 3: TIRF images displaying different frames over time of the same fibre (with a yellow line overlaid as a reference) as it vibrates, appearing at different positions.

Analysis of vibration

In order to analyse the movement of many fibres under identical conditions, we chose a single region (Fig. 3) in a single sample that contains many vibrating fibres that can be compared directly with one another, thereby avoiding region-to-region and sample-to-sample variability. This region with low concentration and interconnection of fibres

in which the fibre vibrations were analysed is shown in Figure 4. In total, eleven fibres were found to be vibrating (highlighted in yellow in Fig. 4 and numbered), but only seven of them were seen clearly enough for the sufficient amount of time to be analysed (fibres 1, 2, 3, 5, 8, 10, 11). To analyse the influence of irradiation on vibrations, three videos of the same region were recorded using different laser intensities: 4%, 6%, and 8% of maximum laser power (Figure S1). The videos that form the basis of the analysis that follows are available in the Supporting Information.

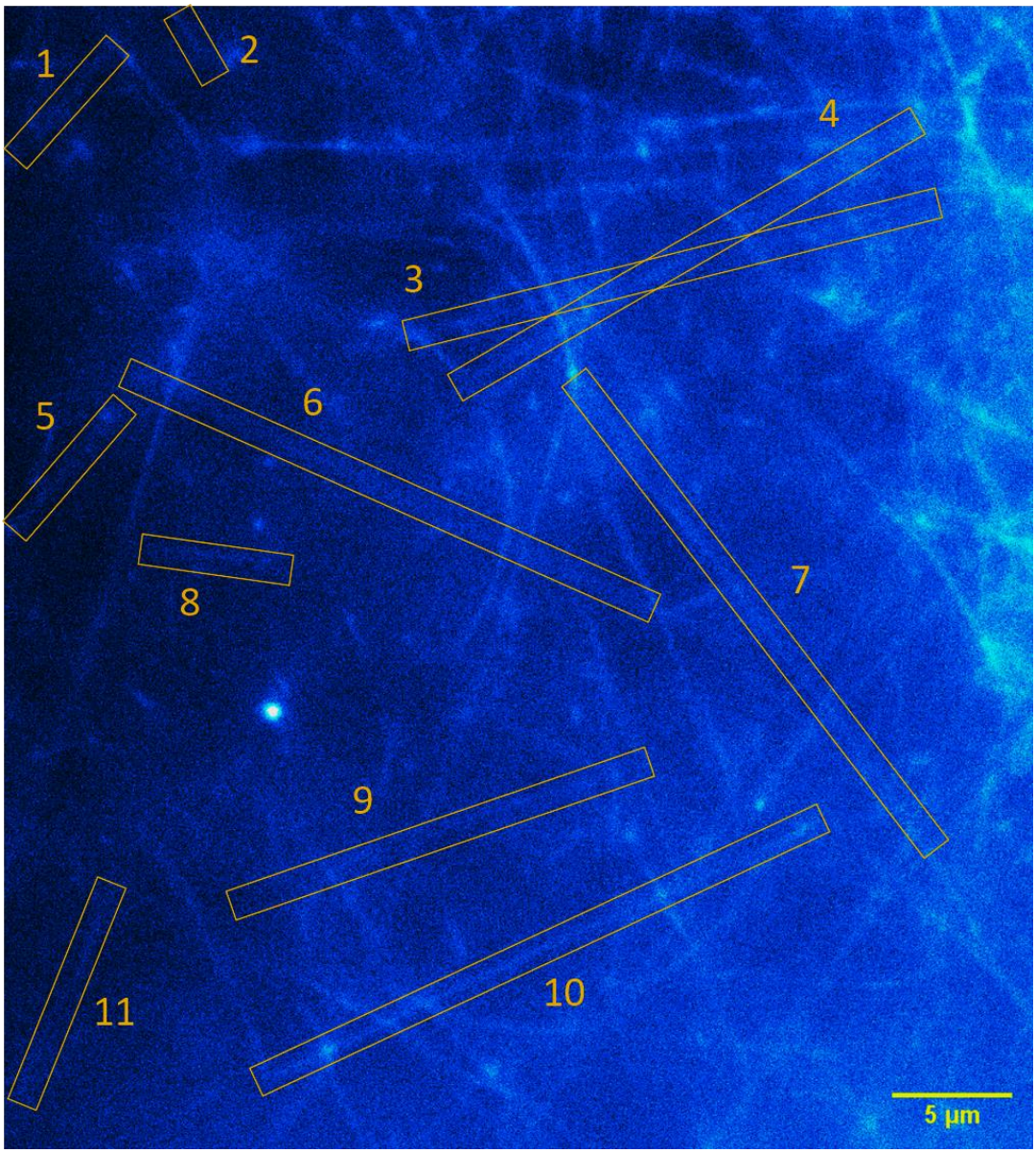

Figure 4: A TIRF image of the **1**·2BrGel@**TCPP**@**Azo** gel in 1:1 water:ethanol (laser intensity 6%, angle 71°) of a low fibre concentration region of the hydrogel where vibrating fibres were observed, with an indication of the fibres used for the subsequent analysis.

As the amplitude of the vibrations was relatively small compared to the resolution of the image (maximum amplitude ranging from 4 to 13 pixels for different fibres compared to average fibre thickness of 7 pixels), and signal to noise ratio was quite

low, manual tracking of the fibre positions was performed. For the tracking, a 2D coordinate system was considered, with the origin lying in the top left corner of the image, and x and y axes oriented to the right and bottom, respectively. For each fibre, a single value of x (or y) coordinate was chosen as fixed (x0; or y0), For each fibre, this value was constant in all three videos. For chosen x0 (or y0), corresponding value of y or x coordinate (yn; or xn, where n is the number of the frame in the video) was determined in the individual frames according to where the x0 (or y0) coordinate crossed the middle of the fibre (Fig. 5). For two sets (different time ranges) of one hundred subsequent images, values of yn (or xn) were then averaged to calculate mean position in the y (or x) direction y0 (or x0). The value of the determined coordinate yn or xn was not precise (we estimate a human error of ± 2 pixels), as the spatial resolution of the image was relatively low for these measurements compared with the observed fibre width (7 pixels). Also, fibres moved relatively quickly regarding the time resolution of the video (100 ms exposure time), so the fibre was sometimes blurred complicating the position determination. For each fibre, a point on the fibre where it seems immobile was determined, which gave us xF and yF coordinates. From these values, deviation angle Φ from the mean position (determined by x0 and y0) was calculated for each frame using the expression 1.

$$\Phi = arctg[(x_F - x_0)/(y_0 - y_F)] - arctg[(x_F - x_n) - (y_0 - y_F)]. \quad (1)$$

Graphs depicting the deviation angle during the 100 subsequent images (Fig. 6 for fibre 5, Figures S2 – S7 for fibres 1, 2, 3, 8, 10, 11) show that the vibrations are apparently non-harmonic. Therefore, the fibre's vibration is not characterised by a single vibrational frequency but rather stochastic movement is observed. We do note that the observed movement indicates an apparent stochastic frequency, because,

although fibres are apparently stationary during each microscopy frame capture (exposure of 100 ms), the vibration of the fibre could be at a faster rate than the image capture.

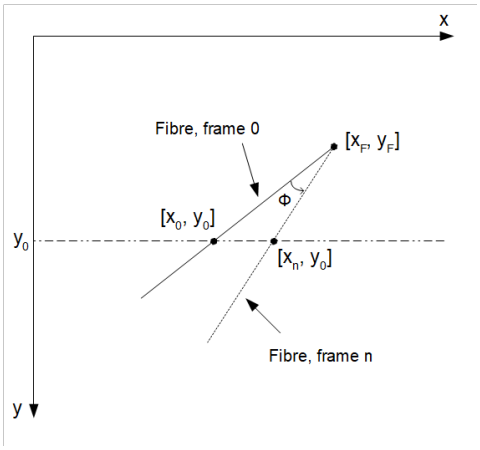

Figure 5: Illustration of the coordinate's determination for the vibrating fibre.

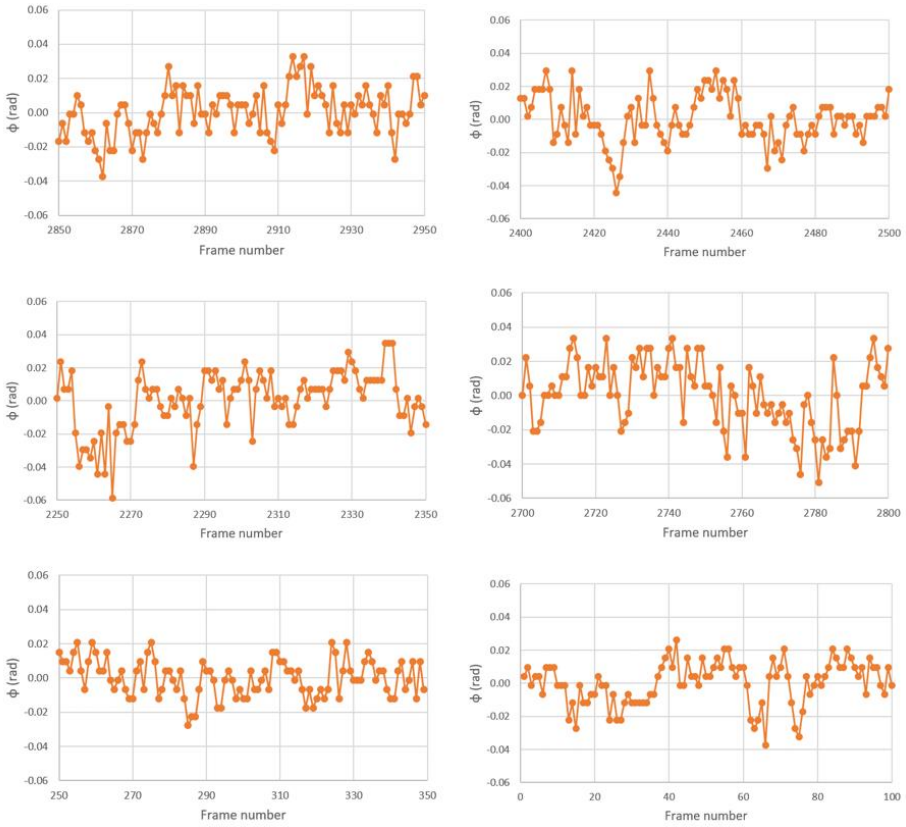

Figure 6: Graphs of deviation angle during 100 subsequent images for fibre 5 in Fig. 4. Deviations measured in the videos recorded with 4% (top), 6% (middle), and 8% (bottom) laser intensity, respectively.

To explore whether the movement could be a result of local heating or other photo-induced effects from the exciting light, the intensity of the laser irradiation was varied. In the graphs used to follow the movement of the fibres, no systematic change in the size of the deviation angle with increasing laser intensity is detected. In order to visualise possible trends in the deviation angle, histograms of the deviation angles for each fibre and laser intensity were plotted (Figures S8 and S9). From visual assessment of the distributions of the angle deviations it follows that there is no clear relationship between deviation angle and laser intensity. For the quantitative evaluation, we calculated the sum of the absolute values of all the deviation angles in the 200 frames corresponding to each fibre and laser intensity, and compared them to

determine the effect of different irradiation power (Table 1). These results indicate that there is no clear dependence of the deviation angle on the laser power in the measured range of the laser intensities.

Therefore, fibre vibrations seem to originate from stochastic thermal motion caused by ambient heat and/or solvent convection in the sample cell. Water and ethanol molecules captured in the gel network move randomly as they possess non-zero internal energy and collide with gel fibres. In case of network with many fibre connections, there are no apparent fibre ends which could have the effect of making the fibre act as a a cantilever. Molecular collision impulse is not sufficient to break fibre connections. However, when the gel network is not well interconnected, there are fibres free on one end. As they are thin, solvent collisions and flow could result in fibre movement which is observed as vibrations. The principle of this motion is the same as in the case of Brownian motion, even though the description of resulting fibre movement would be much more complicated compared to the spherical particle, and because the fibres are connected non-covalently to others at certain points. Therefore, it is expected that temperature increase caused by laser intensity increase will influence speed of the fibre motion. However, as the maximum laser power used was just 8% of maximum intensity, the amount of heat added to the sample was clearly not sufficient to cause any measurable difference in fibre vibrations.

Table 1: Comparison of sum of absolute values of all the deviation angles for 200 images for each fibre at three laser intensities 4%, 6%, and 8%.

Fibre	LI (%)	Sum |Φ| (rad)
1	4	2.712
	6	3.197
	8	2.786
2	4	20.797
	6	24.473
	8	18.607
3	4	1.527
	6	1.520
	8	1.614
5	4	2.270
	6	3.038
	8	1.947
8	4	5.248
	6	4.333
	8	6.682
10	4	0.674
	6	0.828
	8	0.563
11	4	1.902
	6	2.741
	8	1.998

Important to note is that in the analysed region, no **TCPP** movement along the gel fibres was observed, that was seen in other regions of the samples as before [16]. As the local structure in the analysed region is different from the gel structure where **TCPP** movement along the supramolecular fibres is normally observed, we believe that this environment does not favour **TCPP** molecular displacement.

Conclusion

Vibrations of self-assembled fibres of a multicomponent hydrogel were observed in the region of the material where the number of fibres per unit volume is relatively low, resulting in few interconnections between the fibres. Under the conditions used to form these hydrogels, inhomogeneity in the fibre network is frequent, and while these low fibre concentration areas are few, they were always observed in the conditions employed. Video micrographs of fibre vibrations at three laser intensities recorded using the TIRF technique in the same region of the sample show that the movements are robust over the timescale of the experiments (about 5 minutes), meaning that the fibres are not broken or rearranged. Analysis of the videos showed that the vibrations are non-harmonic and their frequency and amplitude are independent of laser power in the measured range. Therefore, the effect does not seem to be a result of photoexcitation. Rather, we conclude that the fibre vibrations result from ambient thermally-promoted motion and/or convection of the fluid around the fibres. This solvent movement around the fibres causes the weakly held objects to move in a random way, with breaking and re-forming of the interconnections between crossing fibres. Therefore, this kind of fibre movement should be present in all regions of this kind of gel with low fibre interconnection.

Although – to the best of our knowledge – this kind of fibre movement has not been reported before, this process is surely happening in many supramolecular and other gels where fibres have relatively few supramolecular crosslinks (fibre-fibre contacts) compared with the bulk of the samples. The observation of the process by TIRF provides an opportunity to study dynamics of inter-fibre interactions and may lead to new insights into the nature of these nanoscopic supramolecular materials.

Experimental

Materials

Ethanol was purchased from PanReac (99.8% HPLC grade), MilliQ water was obtained from a Milli-Q Plus system from Millipore. Sodium hydroxide was purchased from PanRec (98%). 4-(Phenylazo)benzoic acid (**Azo**) (trans:cis ratio of 90:10) and 5,10,15,20-tetrakis(4-carboxyphenyl)porphyrin (**TCPP**) (75%) were purchased from Sigma-Aldrich. 1,3-Bis[(3-octadecyl-1-imidazolio)methyl]benzene dibromide (**1**·2Br) was synthesized using the previously reported procedure [25].

Preparation of Gels

An aqueous solution of the **TCPP** sodium salt (1.2 mM) was prepared by dissolving **TCPP** (4.4 mg, 5.56 µmol) in MilliQ water (5 ml) incorporating sodium hydroxide (22.26 µmol from 0.01 M stock solution). An ethanolic solution of **1**·2Br (200 µL, 40 mM) was mixed with 4-(phenylazo)benzoic acid ethanolic solution (50 µL, 40 mM) and diluted in ethanol to 0.5 mL. The **TCPP** solution (50µL) was diluted in MilliQ water (0.5 mL) together with NaOH (4 mM). Then, the aqueous solution of **TCPP** (0.5 mL) was mixed with the ethanolic solution of **1**·2Br and **Azo** (0.5 mL), pipetted into the CELLVIEW cell culture slide well, sealed with plasticine, and left undisturbed to allow gel formation, which occurs on the order of a few minutes. The final concentrations of **1**·2Br, **TCPP**, and **Azo** were 8 mM, 45 µM, and 2 mM, respectively, while the volume ratio of water:ethanol was 1:1. Samples were prepared at 23 °C.

Methods

Fluorescent imaging was performed on an Andor Dragonfly 505 super-resolution confocal microscope at the Molecular Imaging Platform at the Barcelona Institute of Molecular Biology (IBMB-CSIC). The microscope is equipped with the Fusion acquisition software, fitted with a CFI Apochromat TIRF 100XC Oil objective lens (numerical aperture 1.49) operating in Total Internal Reflection Fluorescence (TIRF) mode (penetration depth 60 nm). A droplet of Nikon Immersion oil type F2 (1.518) was cast on the objective before the imaging. Excitation was performed with 405 nm laser light and emission was recorded using a filter (698 ± 77 nm). For the sample observation using still images, a laser power of 2% was employed, while for the video acquisition, the laser intensity was either 4%, 6%, or 8%. The measurable laser power in wide-field mode using the same configuration was 0.35 mW, 0.47 mW, and 0.60 mW for 4%, 6%, and 8% laser intensity setting, respectively, in the microscope. For the videos, 3000 images were recorded, with 100 ms exposure time (zero gap between frames). The microscope is fitted with a scientific CMOS camera to record each video. Videos were processed using the Fiji image analysis software [26].

Supporting Information

Supporting Information File 1:

File Name: Article BJNANO_DD_nanoscale vibration SI

File Format: .pdf

Title: SUPPORTING INFORMATION for Vibrations of organic nanofibres in a solvated bis-imidazolium supramolecular hydrogel

Supporting Information File 2: Video of fibre motion at 4 % laser power

File Name: Intensity-4p-10fps

File Format: mp4

Title: Video of fibre motion at 4 % laser power

Supporting Information File 3: Video of fibre motion at 6 % laser power

File Name: Intensity-6p-10fps

File Format: mp4

Title: Video of fibre motion at 6 % laser power

Supporting Information File 4: Video of fibre motion at 8 % laser power

File Name: Intensity-8p-10fps

File Format: mp4

Title: Video of fibre motion at 8 % laser power

Acknowledgements

We warmly thank Tania García-Becerra at the Molecular Imaging Platform at the Barcelona Institute of Molecular Biology (IBMB-CSIC) for assistance with the microscope.

Author contributions

Daniela Dupkalová: experimental research, analysis; writing - first draft & editing. David B. Amabilino: conceptualization; methodology formal analysis; funding acquisition; writing – review & editing. Lluïsa Pérez-García: conceptualization; methodology formal analysis; funding acquisition; writing – review & editing.

Funding

We thank the MICIU/AEI/10.13039/501100011033 for financing projects PID2021-123873NB-I00 and PID-2023-146658NB-C32 as well as the "Severo Ochoa" program for Centre of Excellence CEX2023-001263-S. DD thanks the Agència de Gestió d'Ajuts Universitaris i de Recerca (AGAUR) for a predoctoral Joan Oró contract (2024 FI-1 00769).

References

1. Draper E. R.; Adams, D. J. *Chem*, **2017**, *3*, 390-410.

2. Amabilino, D. B.; Smith, D. K.; Steed, J. W. *Chem. Soc. Rev*., **2017**, *46*, 2404-2420.

3. Smith, D. K.; *Soft Matter*, **2024**, *20*, 10–70.

4. Banerjee, S.; Das, R. K.; Maitra, U.; *J. Mater. Chem*., **2009**, *19*, 6649–6687.

5. Skopinska-Wisniewska, J.; De la Flor, S.; Kozlowska, J.; *Int. J. Mol. Sci*., **2021**, *22*, 7402.

6. Sánchez-Fernández, J. A.; *Polymers*, **2023**, *15*, 1365.

7. Ilyas, M. Imran, S. Khan, M. A. Ahmad, Z. Ihsan, A. Qadir, S. Saba, A.; *J. Mol. Liq.*, **2024**, *401*, 124629.

8. Yamada, S.; Honda, T. *ACS Mater. Au*, 2025, 5, 35−44.

9. Lin, D.; Huang, Y.Q.; Qian, Y.; Shen, J.L.; Wei, H.Y.; *J. Mater. Chem. B*, **2026**, *14*, 2999–3022.

10. Terech, P.; Weiss, R. G.; *Chem. Rev*.; **1997**, *97*, 3133-3159.

11. Du, X.W.; Zhou, J.; Shi, J. F.; Xu, B.; *Chem. Rev*., **2015**, *15*, 13165-1307.

12. Nakamura, K.; Kubota, R.; Aoyama, T.; Urayama, K.; Hamachi, I.; *Nat. Commun*., **2023**, *14*, 1696.

13. Wang, R.; Liu, X. Y.; Xiong, J.; Li, J.; *J. Phys. Chem. B*, **2006**, *110*, 7275-7280.

14. Jing, R.; Pennisi, C. P.; Nielsen, T. T.; Larsen, K. L.; *Int. J. Biol. Macromol*., **2025**, *311*, 143461.

15. Dong, R.; Pang, Y.; Su, Y.; Zhu, X.; *Biomater. Sci*., **2015**, *3*, 937-954.

16. Rodrigues, M.; Calpena, A.C.; Amabilino, D. B.; Garduño-Ramírez, M.; Pérez-Garcíca, L.; *J. Mater. Chem. B*, **2014**, *2*, 5419-5429.

17. Limón, D.; Jiménez-Newman, C.; Calpena, A. C.; González-Campo, A.; Amabilino, D. B.; Pérez-García, L.; *Chem. Commun*., **2017**, *53*, 4509-4512.

18. Limón, D.; Talló Domínguez, K.; Garduño-Ramírez, M. L.; Andrade, B.; Calpena, A. C.; Pérez-García, L.; *Colloids Surf. B Biointerfaces*, **2019**, *181*, 657-670.

19. Samperi, M.; Limón, D.; Amabilino, D. B.; Pérez-García, L.; *Cell Rep. Phys. Sci*., **2020**, *1*, 100030.

20. Smith, S. M.; Abelha, T. F.; Limón, D.; Samperi, M.; Sharma, B.; Plaetzer, K.; Dumoulin, F.; Amabilino, D. B.; Pérez-García, L.; *J. Porphyr. Phthalocyanines*, **2023**, *27*, 434–443.

21. Anguluri, K.; Sharma, B.; Bagherpour, S.; Calpena, A. C.; Halbaut, L.; Amabilino, D. B.; Kaur, G.; Chaudhary, G.; Pérez-García, L.; *Photodiagnosis Photodyn. Ther.*, **2025**, *52*, 104529.

22. Samperi, M.; Bdiri, B.; Sleet, C. D.; Markus, R.; Mallia, A. R.; Pérez-García, L.; Amabilino, D. B.; *Nat. Chem*., **2021**, *13*, 1200–1206.

23. Samperi, M.; Pérez-García, L.; Amabilino, D. B.; *Chem. Sci*., **2019**, *10*, 10256–10266.

24. Smith, S. M.; Malagreca, F.; Hicks, J.; Mantovani, G.; Amabilino, D. B.; Parmenter, C.; Pérez-García, L.; *Beilstein J. Nanotechnol*, **2025**, *16*, 2274-2284.

25. Casal-Dujat, L.; Rodrigues, M.; Yagüe, A.; Calpena, A. C.; Amabilino, D. B.; González-Linares, J.; Borràs, M.; Pérez-García, L.; *Langmuir*, **2011**, 28, 2368-2381.

26. Schindelin, J.; Arganda-Carreras, I.; Frise, E.; Kaynig, V.; Longair, M.; Pietzsch, T.; Preibisch, S.; Rueden, C.; Saalfeld, S.; Schmid, B.; Tinevez, J. Y.; White, D. J.; Hartenstein, V.; Eliceiri, K.; Tomancak, P.; Cardona, A.; *Nat. Methods*, **2012**, *9*, 676-682.